Supplementary Information

Anderson Localization of light in a colloidal suspension (TiO_2@Silica)

Ernesto Jimenez-Villar[1], Iran F. da Silva[2], Valdeci Mestre[3, 4], Paulo C. de Oliveira[4], Wagner M. Faustino[2], Gilberto F. de Sá[1]*
[1]Departamento de Química Fundamental, Universidade Federal de Pernambuco, Recife, Pernambuco, 50670-901, Brazil
[2]Departamento de Química, Universidade Federal da Paraíba, João Pessoa, Paraíba 58051-970, Brazil
[3]CCEA, Universidade Estadual da Paraíba, Patos, Paraíba 58706-560, Brazil
[4]Departamento de Física , Universidade Federal da Paraiba, João Pessoa, Paraiba 58051-970, Brazil

Corresponding author: *Ernesto Jimenez-Villar*; E-mail: *Ernesto.Jimenez@uv.es*

Materials and Methods:

Ethanol alcohol HPLC with spectroscopic grade purity was supplied by TEDIA, tetra-ethyl-ortho-silicate (TEOS) was supplied by Sigma-Aldrich, and the ammonia P.A. was supplied by VETEC. The titanium dioxide (TiO_2, nanoparticles of 410 nm) with a rutile crystal structure was acquired from DuPont Inc. (R900). TiO_2 nanoparticles were coated with a silica shell of ~40 nm thickness via the Stöber method. In the first stage, 5 g of TiO_2 Nps were dispersed in 500 ml of absolute ethanol. This suspension was placed in an ultrasound bath for 20 minutes to disperse the particles and 6.67 mL of ammonia and 10 mL of TEOS were added. The TEOS and commercial ammonia (NH_4OH 28%-30%) were added alternately in 100 portions of 100 μl and 220 μl, respectively. The synthesized TiO_2@Silica nanoparticle suspension was rota-evaporated, dried in an oven at 70 °C for 2 h, and re-dispersed in ethanol.

Characterization sample:

Transmission electron microscopy (TEM) and electron-energy-loss spectroscopy (EELS) were performed on a Carl Zeiss Libra 120 kV transmission electron microscope. The commercial carbon-coated Cu TEM grid was immersed in the solution of TiO_2@Silica nanoparticles that had previously been diluted 1000-fold and then left to

dry, before being introduced into the microscope. Figure S1 shows two additional images of the core-shell TiO_2@Silica Nps. It is evident that the silica coating shows great homogeneity, more so than the sample we presented in our previous work.[1, 2] Additionally, the presence of silica Nps with a size of ~40 nm are observable.

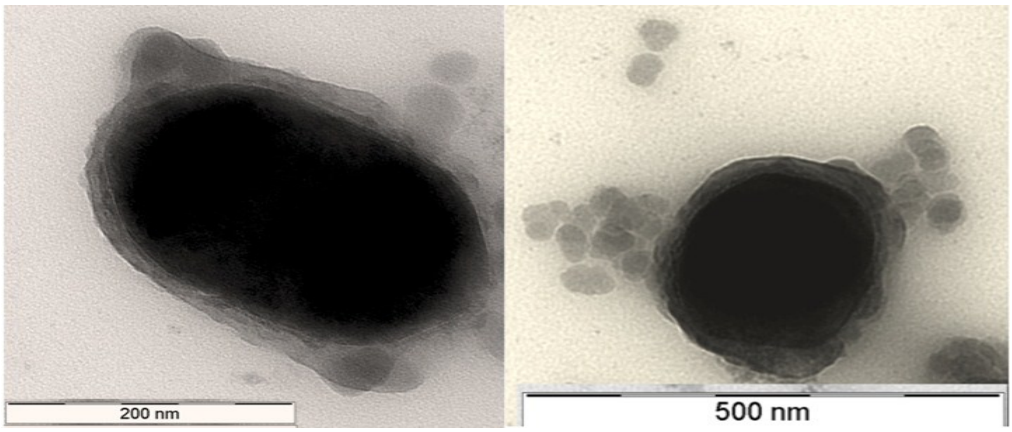

Figure S1. TEM images of core-shell TiO_2@Silica Nps demonstrate the homogeneity of silica shell coating onto the TiO_2 nanoparticle.

For ED-XRF characterization, 200 mg of dried sample powder (TiO_2@Silica) was pressed into a tablet form with a 12 mm diameter. The mass percentage ratio (Ti/Si) of the dried sample powder (TiO_2@Silica Nps) determined by ED-XRF, was Ti_{72}/Si_{28}, which represents an average silica shell thickness of ~42 nm.

Transport experiments

Coherent-ballistic transport

For suspensions of five different concentrations (280, 140, 70, 47, and 14; $x10^{10}$ Np ml^{-1}) of TiO_2@Silica Nps in ethanol, the transmitted coherent intensity I_{TC} has been measured as a function of slab thickness. For [Np]≥$47x10^{10}$ Np ml^{-1}, I_{TC} decay more quickly than an exponential (part I). The scattering mean free paths for *d* near to zero (l_{s0}) were determined from the first experimental point (part I) of the coherent transmission curves. [3] For [$280x10^{10}$ Np ml^{-1}], l_{s0} value cannot be determined because

[1] E. Jimenez-Villar, Valdeci Mestre, Paulo C. de Oliveira, Gilberto F. de Sá, *Nanoscale*, **2013**, *5*, 12512-12517.
[2] E. Jimenez-Villar, Valdeci Mestre, Paulo C. de Oliveira, Wagner M. Faustino, D. S. Silva, Gilberto F. de Sá, *Appl. Phys, Lett.* **2013**. *104.* 081909.

the intensity in part I decayed extremely quickly, which prevented a reliable measurement. Figure S2a shows a schematic diagram of the experimental setup for this transport experiment. The laser beam (second harmonic of *Q*-switched Nd:Yag Continuum Minilite II, λ = 532 nm, 1 μJ (1mJ attenuated 10^3 times by neutral density filters), with a pulse width of ~4 ns, and a repetition rate of 10 Hz) was passed through a positive lens L_1 (200 mm focal length), in order to obtain the focus with its waist near the pinhole PH_1 (600μm diameter). The cell consisted of two optical flats (fussed silica, 3.2mm thickness), F, in wedge form; the slab thickness depends on the incidence point of the cell. The laser spot size on the cell is ~0.5 mm. Another pinhole, PH_2 (1200μm diameter), was positioned 80 mm away from PH_1, in order to reduce the diffuse light. Yet another lens, L_2 (50 mm focal length), allowed for focalization on the optical fiber (200μm). The multimode optical fiber (200 μm) was coupled to a spectrometer HR4000 UV-VIS (Ocean Optics) with a 0.36 nm spectral resolution (FWHM). In order to average out laser intensity fluctuations, the transmitted intensity was acquired by integration during 10s (100 laser shots). For this transport experiment, the laser fluence (Nd:Yag, 532 nm) on the samples was constant (1μJ). Several optical neutral filters were introduced in front of the optical fiber, providing a broad dynamic range of detection. In order to reduce the stray light, the fused silica plates (50 mm diameter) that form the wedge cuvette, were glued with opaque silicone glue. The stray light has been measured for all samples at large slab thickness (~1-2 order lower than signal), and it was subtracted to I_{TC} signal for each [Nps].

---

[3] Martin B. van der Mark, Meint P. van Albada, Ad Lagendijk, *Physical Review B* 1988, **37 (7)**, 3575-3592.

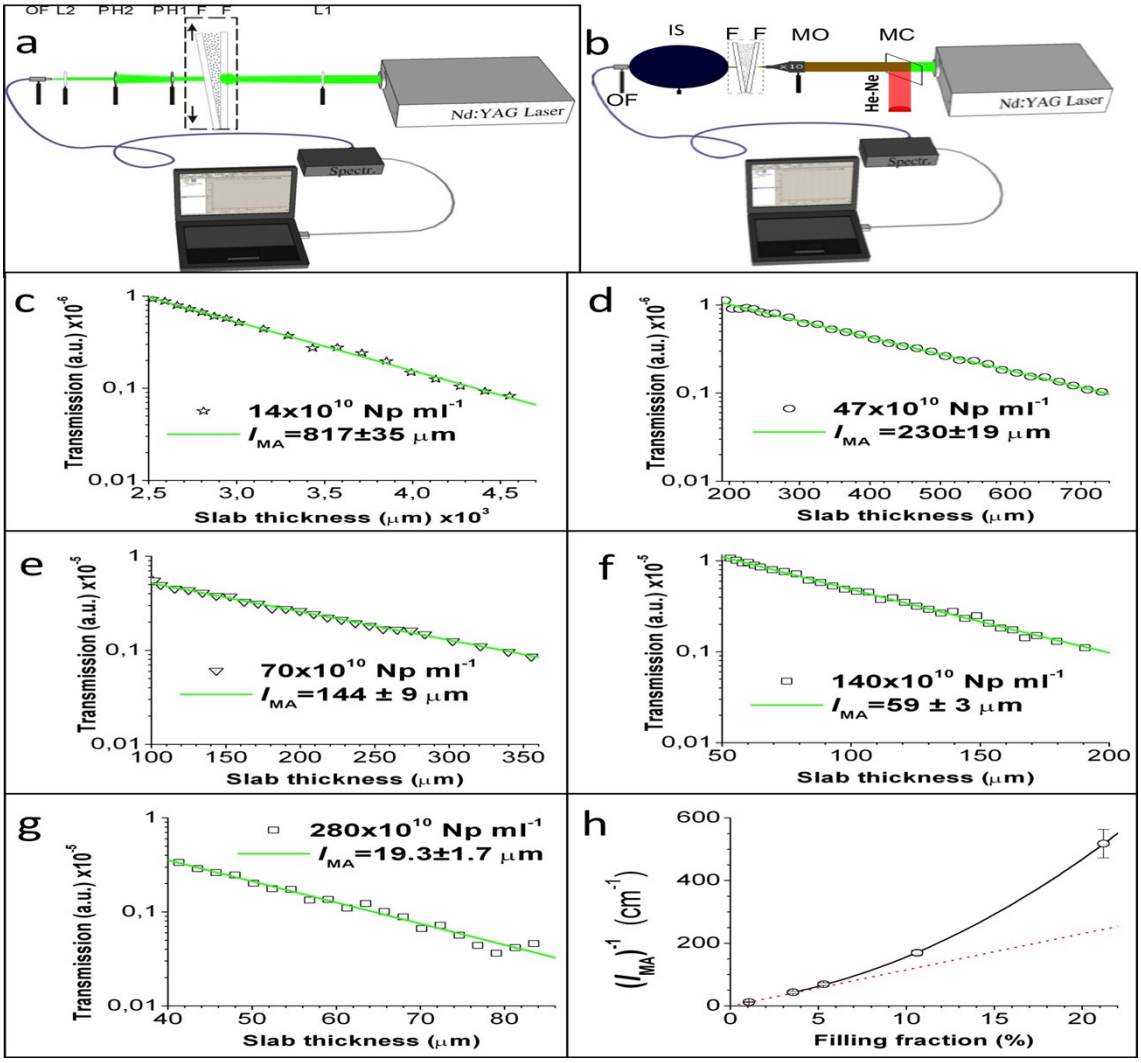

Figure S2. Schematic diagrams of the experimental setup for determination of: a) transmitted coherent intensity as a function of slab thickness. L_1 and L_2, lens; F+F, cell consisting in two optical flat mounted on a translation stage; PH_1 and PH_2, pinholes; OF, optical fiber to collect the light in the spectrometer; b) transmission coefficient, IS, integrating sphere is placed in contact with the back-cell; CW He-Ne (633 nm, 5mW) and pulsed Nd:Yag (532nm, 1μJ) lasers; MO (microscope objective) allows for a spot size <0.5 mm on the cell; MC, microscope coverslip (BK7, 100μm thickness); c-g) Parts III of the coherent transmission curves (measured for 532nm) for [Nps] of: c) 14, d) 47, e) 70, f) 140 and g) 280; x10^{10} Np ml^{-1}. The green lines represent the fitting with an exponential function. h) Inverse of the macroscopic "absorption" length $(l_{MA})^{-1}$ as a function of the filling fraction. The red dotted line represents the expected behavior in the diffusive regime $(C1[FF])$. The black solid line represents the fit with the function $C([FF]-[FF_c])^2 + C1[FF]$.

Figure S2 c-g show the parts III of the coherent transmission curve for [14, 47, 70, 140 and 280; x10^{10} Np ml^{-1}], respectively, whose decay are exponential $\left(e^{-\frac{d}{l_{MA}}}\right)$. From its

inverse slopes, we obtain the macroscopic "absorption" length (l_{MA}). Figure S2h shows the inverse of the macroscopic "absorption" length $(l_{MA})^{-1}$ as a function of filling fraction. As can be observed, $(l_{MA})^{-1}$ increases more quickly than the expected linear increase (red dotted line), which represents an anomalous behavior. The experimental points have been fitted (black solid line) with the following function: $(l_{MA})^{-1} = C([FF] + [FF_c])^2 + C1[FF]$, where C, C1 are constants and $[FF_c]$ can be interpreted as the critical filling fraction for which starts the l_{MA} anomalous behavior. The linear part (C1[FF]) corresponds with the expected linear increase at the diffusive regime. The quadratic term would represent the enhanced "absorption" contribution by localization effect.

[FF] %	1.06	3.5	5.3	10.6	21.2
[Nps] x10^{10} Np ml^{-1}	14	47	70	140	280
l_{MA} values (μm)	817	230	144	59	19.3
l_{s0} values (μm)	11.5	3.4	2.3	1.1	0.55"
L_{T0} values (μm)	13.2	3.9	2.7	1.3	0.65"
l_{In0} values (mm)	50.5	13.6	8	2.7	0.58"
γ_0	1	1.12	1.27	1.84	4.4"
n_{eff} (calculated)	1.37	1.41	1.43	1.53	1.65
l_T (BC) (μm)		0.93	0.7	0.64	0.47
n_{eff0} (enhanced)	1.37	>1.46	>1.55	>1.98	>3.86"
l_{T*} (BC) (μm)		<0.86	<0.6	<0.49	<0.24"

Table S I. l_{MA}, l_{s0}, l_{T0}, l_{In0} and γ_0 values experimentally determinate for each [FF] or [Nps]. Classical n_{eff} (calculated) and enhanced n_{eff0} (estimated by $(n_{eff0} = 1 + \gamma_0(n_{eff} - 1))$ are the effective refractive indexes for each [FF] or [Nps]. l_{T*} (BC) and l_T (BC) are the l_T values extracted from the coherent backscattering cone, with and without the correction of effective refractive index, respectively. The (") symbol represents those values estimated by extrapolation.

From l_{MA} values, we obtain $l_{MA} = (l_T \times l_{In})^{1/2}$, where l_{In} and l_T are the inelastic and transport mean free path, respectively. l_T can be found through $l_T = l_S/(1 - \langle\cos\theta\rangle)$, where $\langle\cos\theta\rangle$ is the average cosine of the scattering angle. The average size of TiO_2 scatter cores (TiO_2@Silica) is 0.41 μm. According to our previous work,[2] the increase of scattering strength by LCE effects in the TiO_2@Silica system is manifested through an

effective increase of the filling fraction, and not by the increase of the scattering cross section. Therefore, assuming scattering cores with a size of 0.41 μm, Mie theory yields a value of 0.13 for $\langle \cos\theta \rangle$, hence, $l_T \approx 1.15 \times l_S$. Table SI shows l_{In} values for d near to zero (l_{In0}) for each [Nps] or [FF]. The "absorption" (l_{In0}^{-1}) per filling fraction (α_{FF0}) must be constant, however, it shows a quadratic increase with [Nps] or [FF] (fig. 2d). This fact must be a consequence of localization phenomenon.

Measurement of transmission coefficient

In order to study the transmitted total intensity, the transmission coefficient was measured as a function of slab thickness. The transmission coefficient is defined as the ratio between the total transmitted flux and the incident flux. The transmitted total intensity is measured with an integrating sphere placed in contact with the back of the cell. Figure S2b shows the schematic diagram of this experimental setup. The pulsed Nd:Yag (532nm) and CW He-Ne (633nm) laser beams were passed through a microscope objective (x20), in order to obtain a < 0.5 mm spot size on the cell. The total transmission is measured with an integrating sphere placed in contact with the back of the sample. The signal was collected through a multimode optical fiber (200 μm), coupled to a spectrometer HR4000 UV-VIS (Ocean Optics) with a 0.36 nm spectral resolution (FWHM). A study of the transmission coefficients for [Nps] of 280, 140, 70, 47 and 14; x10^{10} Np ml^{-1} were performed using both wavelengths (532nm and 633nm) and regimens (pulsed and CW) laser. The fluence of the Nd:Yag laser was ~10^7 times higher than of He-Ne laser. The transmission coefficient shows a $(d_0+d)^{-2}$ behavior for [Nps] ≥47x10^{10} Np ml^{-1}; however, for [14x10^{10} Np ml^{-1}] a classical behavior $(d_0+d)^{-1}$ is observed. Notice that the scattering medium is contained in a fussed silica cell, therefore, the collected intensity must come from angles less than ~42º (respect to perpendicular of cell surface), due to the total internal reflection (silica-air interface).

For [280x10^{10} Np ml^{-1}], this angle would be ~36º because the effective refractive index $n_{eff} \approx 1.64$ (output face). The total intensity (*T(d)*) that would be collected can be expressed by the equation S1 and S2, which correspond to linear and quadratic decay, respectively. ϑ is the collection angle respect to perpendicular of cell surface, ϑ_1 would be the maximum collection angle and *f(ϑ)* is the angular dependence of total intensity. For an ideal case, ϑ_1 is 90º (almost all scattered power is collected), however, in our case, ϑ_1 is ~42º for [Nps] ≤140x10^{10} Np ml^{-1} and ~36º for [280x10^{10} Np ml^{-1}].

$$T(d) = \beta_1^* (d_0 + d)^{-1} \left[2 \int_0^{\vartheta_1} f(\vartheta) d\vartheta \right] \quad \text{S1}$$

$$T(d) = \beta^* (d_0 + d)^{-2} \left[2 \int_0^{\vartheta_1} f(\vartheta) d\vartheta \right] \quad \text{S2}$$

$$\beta_1 = \left[2 \int_0^{\vartheta_1} f(\vartheta) d\vartheta \right] \beta_1^* \quad \text{S3}$$

$$\beta = \left[2 \int_0^{\vartheta_1} f(\vartheta) d\vartheta \right] \beta^* \quad \text{S4}$$

From the equation S1 and S2, it can be determined the linear and quadratic decay that would have *T(d)* if it is integrated over all angle (0º-90º). If β_1 and β are defined by S3 and S4 equation, respectively, it implies that β_1 and β values must be equal for both cases: ideal (0º-90º) and our collection (0º- 42º or 36º). Notice that, for $d \gg d_0$, $T_{\vartheta_1}(d) = \beta_1 / d$ and $T_{\vartheta_1}(d) = \beta / d^2$ for linear and quadratic decay, respectively. However, for ideal collections d_0 must approximately satisfy the relationships S5 and S6 for linear and quadratic decay, respectively. Notice that, for $d \ll d_0$, S1 and S2 equation can be expressed as: $T_{\vartheta_1}(d) = \beta_1 / d_0$ and $T_{\vartheta_1}(d) = \beta / {d_0}^2$, respectively. Additionally, for ideal case

($\vartheta_1 = 90º$), $T_{90º}(0)$ must approximately tend to unity.

$$d_0^{90º} = d_0^{42º} \times T_{42º}(0) \approx d_0^{42º} \times {}^{42º}/_{90º} \approx d_0^{42º} \times 0.47 \quad \text{S5}$$

$$d_0^{90º} = d_0^{42º} \times \sqrt{T_{42º}(0)} \approx d_0^{42º} \times \sqrt{{}^{42º}/_{90º}} \approx d_0^{42º} \times 0.69 \quad \text{S6}$$

For [280x10[10] Np ml[-1]], S6 equation would be; $d_0^{90º} \approx d_0^{36º} \times \sqrt{{}^{36º}/_{90º}} \approx d_0^{36º} \times 0.64$.

Therefore, $T_{42º}(0) \approx 0.47$ (linear decay) and $T_{42º}(0) \approx (0.69)^2 \approx 0.47$(quadratic decay). For [280x10[10] Np ml[-1]], $T_{42º}(0) \approx (0.64)^2 \approx 0.42$. Notice that, the total transmission has been performed with two-laser sources: one pulsed (532nm) and other CW (633nm) with fluencies and wavelengths completely different, however, the quadratic decays are similar. Typically, a sample "absorption" dependency is expected with the wavelength, which would greatly modify the total transmission curves. Additionally, a dependency of the inelastic scattering processes with the fluence must also be expected. However, the total transmission curves for both lasers are similar. For [14x10[10] Nps ml[-1]], transmission coefficient fits very well with a $\beta_1(d_0 + d)^{-1}$ decay. However, for [Nps] ≥47x10[10] Nps ml[-1], the experimental points fit very well with a $\beta(d_0 + d)^{-2}$function. For [Nps] ≤ 140x10[10] Nps ml[-1], the transmission coefficients tend to ~(0.47), which correspond with the expected transmission coefficient for *d*=0. However, for [280x10[10] Nps ml[-1]], the transmission coefficient tends to a value (~0.3) lower than the expected value (~0.42), which must be the result of an increase of the losses due to enhanced "absorption".

In order to estimate the expected transmission curve for [280x10[10] Nps ml[-1]] without "absorption" effect, the experimental points was fitted with $\beta(d_0 + d)^{-2} \times A$ expression, where *A* is a constant that would represent the intensity losses by "absorption". *A* value was fixed such that ${}^{\beta}/_{(d_0)^2} = 0.42$, which is the expected value of transmission

coefficient at d=0. The green dotted line in the figure S3a represents a possible quadratic decay $\left(\beta(d_0+d)^{-2}\right)$ without intensity losses by "absorption" ([280x10^{10} Nps ml^{-1}]). Clearly, the above approach is not strictly correct; it is just a rough approximation in order to find a possible decay behavior without the "absorption" effect. At localization transition complex phenomena can arise, such that the inelastic mean free path could be sensitive to depth and propagation angle. Therefore, a theoretical approach including the interplay between localization and "absorption", and "absorption" dependence with the propagation angle and depth it becomes necessary.

For [Nps] ≥47x10^{10} Nps ml^{-1}, we have also tried to fit the transmission coefficient curve with an exponential decrease rather than a parabolic one, but without success. It fits very well with a $\beta(d_0+d)^{-2}$ function. In any case $T(d)=\beta_1(d_0+d)^{-1}$ function, because it does not fit well and d_0 would be negative, i.e. indeterminate in d_0.

On the other hand, the experimental points were also fitted with $T(d)=\left(l_{MA}^*/\gamma l_T\right)\sinh^2\left(\gamma l_T/l_{MA}^*\right)/\sinh\left(d/l_{MA}^*\right)$, γ=5/3 function, which is derived from diffusion theory with absorption in the crossover region. [4] $l_{MA}^* \approx l_{MA}/\sqrt{B}=\left(l_T\times l_{In}/B\right)^{1/2}$, where B is the freedom degrees, linked to the solid angle of collection. As only the scattered energy with angles <(±42º or 36º) is collected, the freedom degrees are reduced to ~(1.9 or 1.8). The black dotted lines in the figure S3a show the fitting with the above expression. For [14x10^{10} Nps ml^{-1}], this fit is insensitive to $l_{\mathrm{MA}*}$ ($l_{\mathrm{MA}*}$ ~∞), which means that the experimental points must not be in the crossover region. Notice that, $\left(l_{MA}^*/\gamma l_T\right)\sinh^2\left(\gamma l_T/l_{MA}^*\right)$ term would be around 10^{-2}, therefore, it would be negligible in the measurement range. The $\boldsymbol{l_T}$, $\boldsymbol{l_{MA*}}$ and $l_{MA}=l_{MA}^*\times\sqrt{B}$ values extracted through the last fitting are displayed in the table SII. As can be observed, these values are much higher

[4] Scheffold, F., Lenke, R., Tweer, R. & Maret G. Localization or classical diffusion of light? *Nature* **398**, 206 (1999).

than those determined by the coherent backscattering cone or ballistic transport. Additionally, the $\boldsymbol{l_{MA^*}}$ and $\boldsymbol{l_{MA}}$ values also show an anomalous behavior, it shows a $(l_{MA})^{-1} = C([FF] + [FF_c])^2 + C1[FF]$ dependence. Therefore, the diffusion theory with absorption could not explain the anomalous decay of the total transmission for [Nps] ≥47x10^{10} Nps ml^{-1}. The green and red solid lines (fig. S3a) are fitting with experimental points by using the quadratic decay function ([Nps] ≥47x10^{10} Nps ml^{-1}) and the linear decay function ([14x10^{10} Nps ml^{-1}]) for Nd:Yag and He-Ne lasers, respectively. We must highlight that the β fitting parameter $(\beta(d_0 + d)^{-2})$ also decreases quadratically in [Nps] (fig. S3b), being more pronounced for 633nm (He-Ne) laser. A $\beta^{-1} = C_0 + C_1([N_{ps}] - [N_c])^2$ dependence was found, where C_0, C_1 are constants and $[N_c]$ can be interpreted as the critical [Nps] which starts the β parabolic dependence.

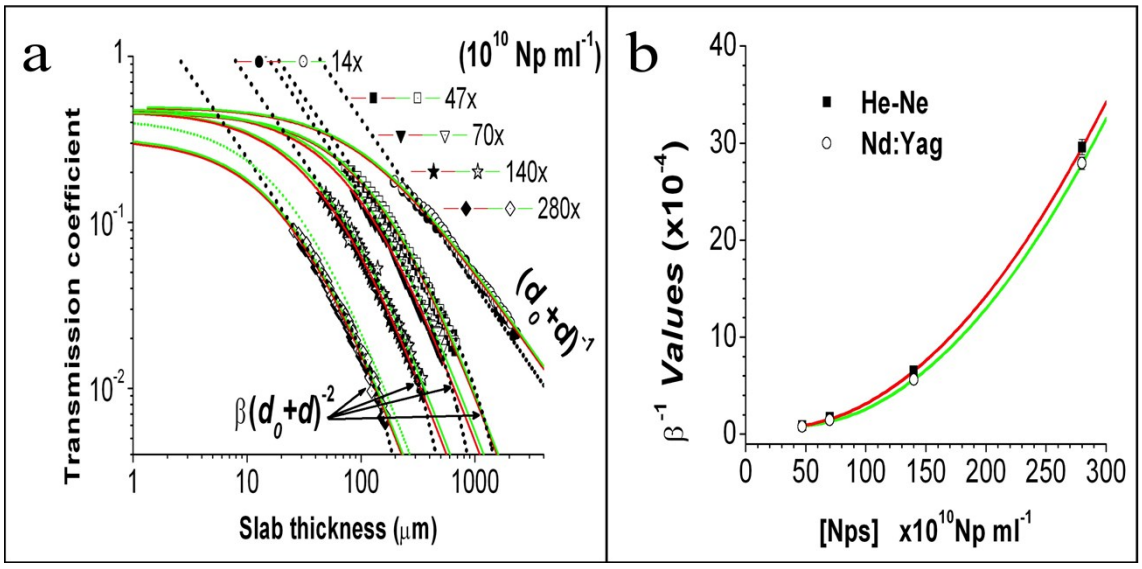

Figure S 3. a) Transmission coefficient for the lasers: pulsed Nd:Yag and CW He-Ne and [Nps] of: 14, 47, 70, 140 and 280; x10^{10} Nps ml^{-1}. Open and filled symbols correspond to experimental points for Nd:Yag and He-Ne (lasers), respectively. Green and red solid lines represent the fitting with experimental points ($(\beta(d_0 + d)^{-2}$ or $\beta_1(d_0 + d)^{-1}$) for Nd:Yag and He-Ne (lasers), respectively. The green dotted line [280x10^{10} Nps ml^{-1}] corresponds with a possible transmission curve without "absorption" contribution for Nd:Yag laser. The black dotted lines are derived from diffusion theory with absorption $T(d) = (l^*_{MA}/\gamma l_T)\sinh^2(\gamma l_T/l^*_{MA})/\sinh(d/l^*_{MA})$, γ≈5/3. b) β^{-1} evolution shows a quadratic increase as [Nps] is increased. Closed squares (red line) and open circles (green line) correspond to β^{-1} evolution for He-Ne and Nd:Yag lasers,

respectively.

[FF] (%)	1.06	3.5	5.3	10.6	21.2
[Nps] (x10^{10}Np ml^{-1})	14	47	70	140	280
l_T (μm)	12.3	5.4	4.5	2.2	0.8
l_{MA*} (μm)	Insensitive (∞)	500	253	137	62
l_{MA} (μm)	-	689	349	189	83

Table S II. l_T and l_{MA*} values extracted through the fitting with the crossover function $T(d) = \left(l_{MA}^*/\gamma l_T\right)\sinh^2\left(\gamma l_T/l_{MA}^*\right)/\sinh\left(d/l_{MA}^*\right)$. The l_{MA} values were calculated through $l_{MA} = l_{MA}^* \times \sqrt{B}$ expression.

Propagation experiment

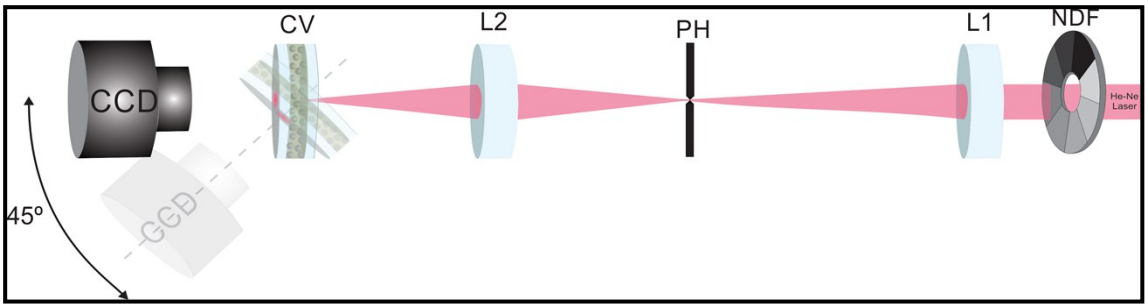

Figure S 4. Schematic diagrams of the experimental setup for determination of the intensity profile after propagating through samples, L_1 and L_2, lens; PH, pinhole; CV, fussed silica cuvette of ~1.8 mm optical pathlength; CCD camera; NDF, neutral density filter.

The intensity structure of a He-Ne beam was studied after propagating a distance of ~1.8 mm through the samples. Figure S4 shows a schematic diagram of the experimental setup for this study. The probe beam (He-Ne laser), linearly polarized, was passed through a positive lens L_1 (200 mm focal length), in order to obtain the focus with its waist near the pinhole PH (600μm diameter). Another lens, L_2 (38 mm focal length), was positioned 250 mm away from PH, in order to focalize the beam on the cell, CV. The spot size on the input face of the sample is less than 100μm. Neutral density filters were used to attenuate the beam intensity (He-Ne). The cell consisted of two optical flats (fussed silica, 3.2 mm thickness), the optical pathlength was 1.8 mm. In order to reduce the stray light, a metallic film with an aperture of ~5 mm diameter, through which the probe beam enters, is placed in the input interface silica-sample. A

CCD camera collected the images of probe beam at output face. The probe beam was introduced with incidence angles of 0º, 30º, 45º and 60º regarding to normal incidence. The beam polarization is parallel to incident plane. The confinement of the beam at the output plane is quantified by the inverse participation ratio $P \equiv \left[\int I(x,y)^2 dxdy\right] / \left[\int I(x,y) dxdy\right]^2 = \frac{1}{\pi}\left[\int_{-\infty}^{+\infty} I(r)^2 dr\right] / \left[\int_{-\infty}^{+\infty} I(r) dr\right]^2$, which has units of inverse area, and an effective width $\omega_{eff} = (P)^{-1/2}$. The statistical standard deviation of P (ΔP) is determined by $\left(\frac{1}{\pi}\sqrt{\left(\frac{d[P(r)]}{dr}\right)^2} \times unit\ distance\right)$ evaluated in $r \approx 0$. Notice that, for a symmetric function regarding to *r*=0 (like the intensity profiles), *P* operation over *I(r)* yields a monotonic decreasing function with an inflection point at *r*=0. *P* variance is defined as the moment of second order, which can be determine through its derivative $\left(\frac{1}{\pi}\sqrt{\left(\frac{d[P(r)]}{dr}\right)^2}\right)$ in the inflection point (*r*=0) because the higher order derivative are zero (symmetric function).

Measurement of transport mean free path by backscattering method

In order to determine scattering strength by another way, the coherent backscattering cones were measured for [47, 70, 140 and 280; x10^{10} Np ml^{-1}]. Figure S5a shows the experimental setup to measure the backscattered light. The laser beam (He-Ne), linearly polarized, was passed through a positive lens L_1 (200 mm focal length), in order to obtain the focus with its waist near the pinhole PH (600μm diameter). Another lens, L_2 (150 mm focal length), was positioned 150 mm away from PH (focal length), in order to collimate the beam on the cell, CV. The sample is illuminated through a beam splitter that reflects 50% of laser intensity. The light backscattered is collimated by a lens L_3 (25 mm focal length) and a CCD collects it. Neutral density filters were used to attenuate the beam intensity (He-Ne). The cell is composed of two fused silica optical

flats (6 mm thickness). In order to average out the speckle pattern, the collection time was 500 seconds, which is enough for particle diffusion in the suspension. The sample was slightly tilted (horizontal) to keep the specular reflection from reaching the detector.

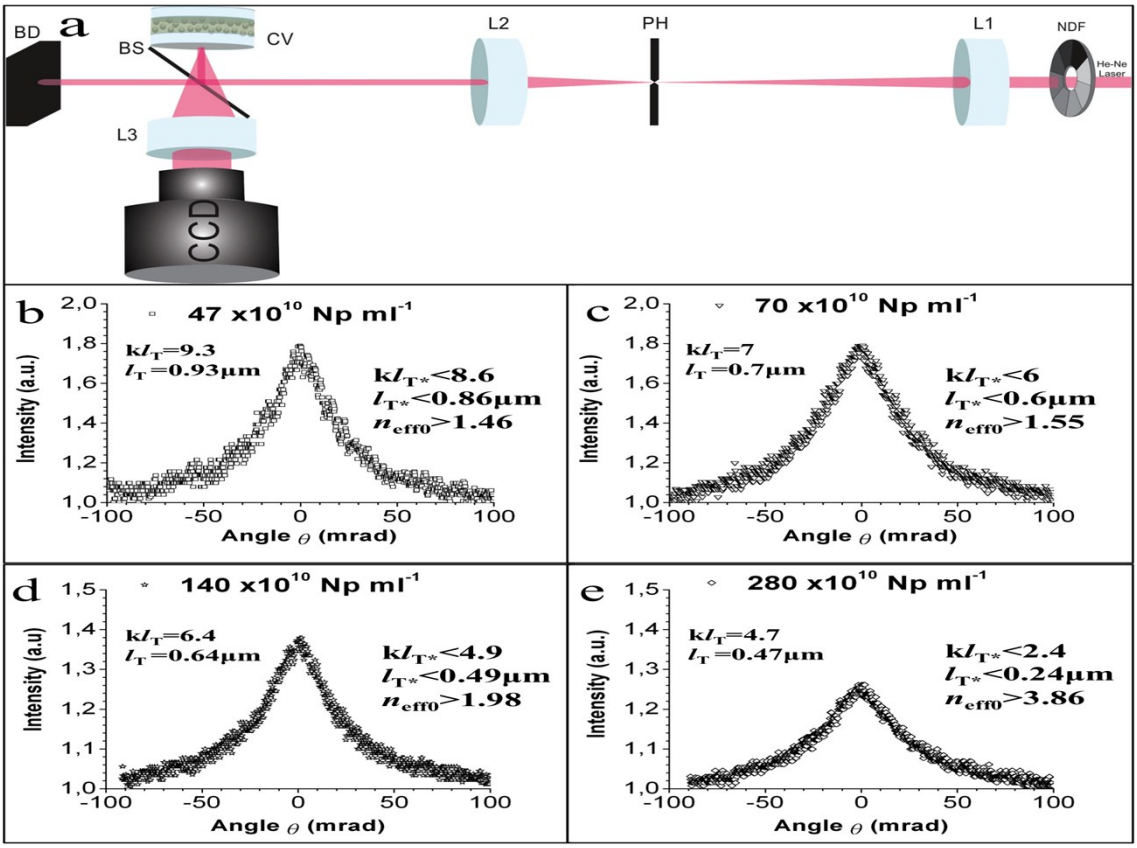

Figure S 5. a) Experimental setup for determine the coherent backscattering cone, L_1, L_2 and L_3, lens; PH, pinhole; BS, beam splitter; CV, cuvette of 2 mm optical pathlength; CCD camera; BD, beam dump. b,c,d,e) coherent backscattering cones for [Nps] of: b) 47x10^{10} Np ml^{-1}, c) 70x10^{10} Np ml^{-1}, d) 140x10^{10} Np ml^{-1}and e) 280x10^{10} Np ml^{-1}. kl_{T*} and kl_T were determined with and without the refractive index correction, respectively. The enhanced effective refractive indexes at d near to zero are also displayed inside. The intensity is normalized by the background intensity of backscattering.

Figure S5 (b,c,d,e) shows the backscattering cones for [47, 70, 140 and 280; x10^{10} Np ml^{-1}], inside are displayed the values of kl_T, l_T, kl_{T*} and l_{T*} extracted by this method. Notice that for [140 and 280; x10^{10} Nps ml^{-1}], low enhancement factors are observed in the backscattering cones. This fact could be caused by the total internal reflection of coherently backscattered photons in the input interface sample-silica. The latter would

have an important connotation. Notice that for [140 and 280; x10^{10} Nps ml^{-1}], the effective refractive index (enhanced), that "feels" the coherently backscattered photons, is much higher than the silica refractive index. So, the coherently backscattered photons at large angles would suffer a total internal reflection at the interface sample-silica. Therefore, only the incoherently backscattered photons, that “feel” a classical refractive index, would be detected for large angles. In this way, the background intensity (backscattering) must increase. For [280x10^{10} Nps ml^{-1}], half angle of the coherent backscattering cone, without the correction by internal reflection, would be ~220 mrad. However, the angle of total internal reflection in the interface sample-silica would be ~380 mrad. Therefore, a significant part of the coherently backscattered light would be forced to come back to the sample, contributing consequently to the background of backscattering. A simple model for internal reflection was taken account for correction of l_T values.[5] The effective refractive index should increase at least as $(n_{eff0} = 1 + \gamma_0(n_{eff} - 1))$ for d near to zero, since the photon would interact an average γ_0 times with the same particles, atoms or molecules. Notice that, the proposed increase in the effective refractive index is connected with the known Kramers-Kronig relations, due to $\alpha_{FF0}(\omega) = \gamma_0 \times \alpha_0(\omega)$. Thereby, $n_{eff0}(\omega_0) = 1 + \gamma_0(n_{eff}(\omega_0) - 1)$. The enhanced effective refractive indexes at d near to zero (n_{eff0}), extracted by scaling through the enhanced absorption factor $(n_{eff0} = 1 + \gamma_0(n_{eff} - 1))$, are also displayed inside (fig. S5). This effect could be interpreted such that the photons interact an average of γ_0 times (at d near to zero) with the same particles, atoms, or molecules, leading to an increase of γ_0 times in the elastic polarization of valence electrons to virtual states. Figure S6 shows the evolution of l_{T0}, l_T and l_{T*} as a function of [Nps]. As can be observed, l_{T0} shows a linear decay in [Nps] ($l_{T0} \propto$ [Nps]$^{-1}$). However, l_T and l_{T*} decay more slowly. This fact

[5] Ad Lagendijk, Rob Vreeker, Pedro de Vries, *Physics Letters A* **1989**, Vol. **136 (1-2),** 81-88.

could mean that, effectively, a n_{eff0} correction is required and that n_{eff0} must increase even more just at d=0 (input interface silica-sample). Notice that, the l_{s0}, l_{T0} and α_{FF0} are average values determined in the region at d near to zero, not at d=0, where these values must increase even more. Consequently, a further increase in the effective refractive index must be expected at d=0. Additionally, the enhanced factor of coherent backscattering cone is lower than expected (~1.8) for [Nps] ≥ 140x10^{10} Nps ml^{-1}, which could introduce an error in estimating the backscattering cone angle. By this reason n_{eff0} values have been succeeded by (>) sign in the figure S5 b-e. In this way, a new theoretical approach would be required in order to consider the total internal reflection, by localization effects, in the input interface sample-silica.

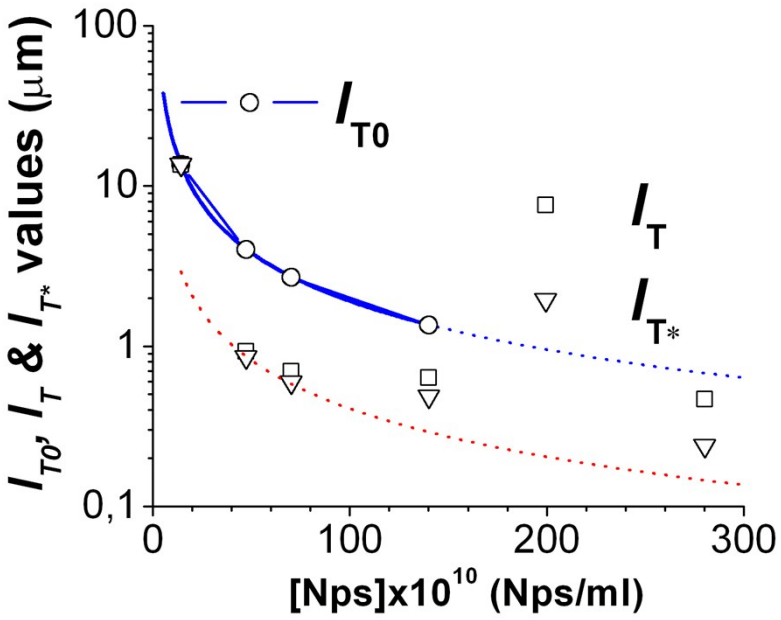

Figure S 6. Evolution of l_{T0}, l_T and l_{T*} as a function of [Nps]. The blue and red dotted lines represent the fitting with inverse functions ([Nps]$^{-1}$). The red dotted line shows the expected $l_{T*} \propto [N_{ps}]^{-1}$ dependence for [Nps] ≥ 47x10^{10} Nps ml^{-1}.